Magnetization reversal in (100) Fe thin films

J. M. Florczak and E. Dan Dahlberg

School of Physics and Astronomy, University of Minnesota, 116 Church Street S.E., Minneapolis, Minnesota 55455

(Received 19 April 1991)

The longitudinal and transverse magneto-optical Kerr effects have been used for understanding the magnetization processes in single crystal Fe/GaAs (100) thin films. By using both of these Kerr effects it is possible to concurrently detect two orthogonal in-plane magnetization components. Presented here are Kerr hysteresis curves for magnetic fields directed along the in-plane $\langle 100 \rangle$ and $\langle 110 \rangle$ directions of the Fe films. For the $\langle 100 \rangle$ direction the magnetization curves are square, while for the $\langle 110 \rangle$ unusual overshoots are present in the Kerr hysteresis curves. In order to understand the origin of these curves for the $\langle 110 \rangle$ direction, simulations were done using the Fresnel reflection coefficients for the in-plane Kerr effects and a coherent-rotation model for the magnetization process. There is good agreement between the simulated Kerr hysteresis curves and the experimental data. The overshoots along with the general analyzer dependence of the hysteresis curves are reproduced in the simulations. However, the magnitude of the reversal and saturation fields of the modeled loops cannot be brought into agreement with the data. For applied fields near the $\langle 110 \rangle$ directions, the analysis suggests that the reversal occurs through the nucleation and/or unpinning of 90° domains at two distinct transition fields followed by coherent rotation.

I. INTRODUCTION

Since 1926 when Honda and Kaya[1] published the magnetization curves for the principal crystal axes in bulk Fe, the properties of Fe have been exhaustively studied both in single-crystal and polycrystalline systems.[2,3] As one can imagine, given the ubiquity of hysteresis curves, a considerable effort has been,[4] and continues to be,[5] devoted to interpreting the magnetization processes responsible for the shapes of hysteresis curves. For the case of a single crystal, the magnetization process can be described in a rather straightforward manner. This is done, regardless of how complex the process may be, by indicating the direction of the magnetization as a function of the applied magnetic field. For polycrystalline materials one can still denote the direction of the magnetization within a crystallite, but the magnetization curve is now a result of an average over the various processes occurring in the differently oriented crystallites. Thus it is important to understand the fundamental magnetization processes that occur in single crystals before grappling with more complex systems. However, even bulk single crystals have complications. As an example, demagnetizing effects can alter both the magnitude and direction of the magnetic field within the sample. By virtue of these effects, it is not certain that the internal field will be the same as the applied magnetic field. Shaping crystals into certain forms, such as those with calculable demagnetizing factors, can alleviate this problem. However, for the magnetization process itself, the number of modes in which the reversal can take place in bulk crystals inherently restricts the interpretation of the hysteresis curves. Johnson and Brown,[6] in an early study, pointed this out as the limitation in their static-energy calculations of hysteresis loops for bulk Fe crystals.

One possible recourse is to examine single-crystal films. For a thin film made from a magnetic material with relatively low crystal anisotropy, low compared to $4\pi M_s$, the foregoing problem is eliminated as a result of the demagnetizing field which effectively confines the magnetization to reverse in the film plane. Furthermore, with the introduction of molecular-beam epitaxy (MBE), it is now possible to prepare single-crystal Fe films with rather unique properties. As an example, the predicted first-order phase transition in the magnetization of Fe in an applied field was experimentally observed in Fe/GaAs (110) films by Hathaway and Prinz.[7] These points are some of the motivating factors for the present study of the magnetization reversal in Fe/GaAs (100) thin films. It should be pointed out that although the magnetic and structural properties of Fe/GaAs films were the focus of recent experimental investigations,[8-13] there has not been a detailed study of the magnetization processes in these systems.

Two points make the Fe/GaAs (100) thin films attractive to study over bulk crystals. First, as mentioned before, because of the demagnetizing fields of the thin-film geometry, the magnetization is effectively forced to lie in plane. This constraint drastically reduces the possible modes for reversal and, hence, simplifies the interpretation of the magnetization curves. With simple models, coherent rotation for example, considerable insight can be gained into how the reversal proceeds within the complex anisotropies of an Fe film. As a followup on the last point, previous studies[14] of the ferromagnetic resonance (FMR) properties of these films indicated a notable uniaxial anisotropy. This anisotropy effectively reduces the symmetry of the (100) plane, making the two in-plane $\langle 110 \rangle$ directions inequivalent. For films of approximately 100 Å thickness, it was found that this uniaxial term was ~17% of the fourth-order magnetocrystalline an-

isotropy. How this uniaxial term affects the magnetization process in a cubic anisotropy field has not been addressed.

Presented here are the results of a systematic study of the magnetization processes in Fe/GaAs (100) films using magneto-optical Kerr effects. The Kerr-effect technique is particularly suited for examining the magnetization reversal in thin films. For in-plane magnetization, the longitudinal and transverse Kerr effects can be used to sense simultaneously or individually two orthogonal components of the magnetization.[15] This sensitivity to two magnetization components yields a basic advantage over single-component detection schemes by being able to track the direction of the magnetization vector.

The immediate discussion focuses on the magnetization processes for magnetic fields along and near the in-plane $\langle 110 \rangle$ and $\langle 100 \rangle$ directions. In the case of the $\langle 110 \rangle$ direction, the data along with the simulations suggest a very novel reversal which can be attributed to a disorientation of the applied field from this direction. However, the simulations cannot reproduce the reversal and saturation fields simultaneously. On the basis of the analysis, it is reasonable to conclude that the reversal occurs by the nucleation or unpinning of 90° domains at two distinct fields followed by coherent rotation.

The remaining presentation is organized into five sections. Outlined in Sec. II is a description of the magneto-optical apparatus and Fe films. The rotational model for the magnetization process in the (100) plane of Fe is introduced in Sec. III A. In this section typical Kerr hysteresis curves from the Fe/GaAs (100) systems are presented for applied fields parallel to the $\langle 100 \rangle$ and $\langle 110 \rangle$ directions. In Sec. III B the relevant magneto-optics is discussed in terms of a mixture of two Kerr effects. The relevance of this unconventional analysis becomes significant when trying to understand the presence, and even absence, of any analyzer dependence in the Kerr hysteresis curves. In particular, the appearance of the two irreversible transitions in the $\langle 110 \rangle$ curve indicates that the magnetization process is more complex than a simple rotation.

A general description of the experimental results is given in Sec. IV. For the $\langle 110 \rangle$ magnetization curve, a reversal of the magnetization comes about by the nucleation or unpinning of 90° domains at two distinct fields followed by rotation. In Sec. V the model is described further and compared to the experimental data. There is good agreement between the experimental and simulated Kerr hysteresis curves. The analyzer dependence is adequately reproduced, even the overshoots, and the two irreversible transitions appear to be a natural consequence of the cubic anisotropy and orientation of the applied field. However, the observed transition fields cannot be sufficiently accounted for by the coherent rotation model. Finally, a summary of the results appears in Sec. VI.

II. EXPERIMENT

The Fe films examined here were deposited onto (100) GaAs by molecular-beam epitaxy. The semi-insulating

(100) GaAs wafers were first prepared by chemically etching in a 6:1:1 solution of $[H_2SO_4]:[H_2O_2]:[H_2O]$ and then heating to 600 °C in vacuum to anneal the GaAs and to remove any surface oxides. In order to further improve the surface of the GaAs, a 1000-Å buffer layer of GaAs was grown on the substrate. After the growth of the GaAs buffer layer, 100–150 Å of Fe were evaporated onto the GaAs at substrate temperatures of 200 °C. Pressures during the Fe deposition were typically 10^{-9} Torr. During the above depositions, the surfaces were monitored by reflection high-energy electron diffraction (RHEED), which, in the final deposition, revealed good epitaxy of the Fe to the GaAs. For the GaAs (100) oriented plane, epitaxy of Fe onto this surface induces the (100) plane of Fe to form. In this plane there are two magnetically easy $\langle 100 \rangle$ and two magnetically intermediate $\langle 110 \rangle$ directions such that the $\langle 100 \rangle$ directions are rotated 45° from the $\langle 110 \rangle$ directions.

The samples were then removed from the vacuum and placed on a rotatable stage between the pole faces of an electromagnet. This sample stage allowed the magnetic field to be oriented at various angles relative to the in-plane crystal axes of the film. For the data reported here, the magnetic field is always applied perpendicular to the plane of incidence of the light beam and in the plane of the film. The incident light from the He-Ne laser was oriented 60° from the sample normal and polarized in the plane of incidence. Last, the hysteresis curves were taken at room temperature with typical sweep rates of the magnetic field of 20 Oe/sec.

III. THEORY

A. Magnetics

For many magnetic materials, part of the magnetization process can be attributed to a rotation of the magnetization.[16] This is particularly true for the magnetically "hard" directions of an anisotropic magnet. There has been evidence that this type of simplistic rotation model can result in good agreement with the magnetization of Fe/GaAs (110) thin films.[17] In light of this, a rotational mechanism for the magnetization reversal is utilized for the Fe/GaAs (100) films. If the thin film is considered to be a single domain of magnetization **M**, then the magnetization curves for a coherent rotation mechanism can be calculated using a phenomenological expansion of the free-energy density. The direction of the magnetization within this domain is determined by the interplay between the anisotropy of the material and the externally applied field. Using the work of Krebs, Jonker, and Prinz[14] and others[9] as a guide, five terms in the free-energy expansion are used to describe the Fe/GaAs (100) films. This free-energy density of a single domain can be expressed as

$$E = K_1[\alpha_1^2\alpha_2^2 + \alpha_1^2\alpha_3^2 + \alpha_2^2\alpha_3^2] + K_2[\alpha_1^2\alpha_2^2\alpha_3^2]$$
$$+ K_u \sin^2\theta + 2\pi M_n^2 - \mathbf{M}\cdot\mathbf{H} . \tag{1}$$

The terms involving K_1 and K_2 represent the magneto-crystalline anisotropy for a system with cubic symmetry such as Fe; the K_j's are the phenomenological anisotropy constants, and the α_i's are the direction cosines of $\mathbf{M}$ in this system. The third term, containing the constant K_u, is a uniaxial anisotropy introduced by Krebs, Jonker, and Prinz[14] to explain their ferromagnetic resonance data on similarly prepared Fe/GaAs (100) systems. In this third term, θ denotes the angle of $\mathbf{M}$ relative to the axis of this anisotropy, which is along one of the two in-plane $\langle 110 \rangle$ axes.

It has been conjectured that the uniaxial term is a result of the preferential orientation of surface irregularities or to an asymmetry in bonding at the Fe/GaAs interface.[14] For the former hypothesis, periodic surface irregularities have been invoked by Schlomann[18] to explain the uniaxial anisotropy of obliquely deposited permalloy films. This uniaxial anisotropy is a result of the demagnetizing effects of the surface roughness in those films. In the Fe/GaAs (100) films, if roughness is the explanation, then by Schlomann's argument the uniaxial anisotropy will have an axis along either $\langle 110 \rangle$ if the surface roughness (suppose they are parallel scratches) has an orientation parallel to a $\langle 110 \rangle$ direction. This type of orientation for the surface irregularities have been observed in Fe/In$_x$Ga$_{1-x}$As/GaAs (100) systems.[19] The observed corrugations in these films are due to the strain relaxation of the In$_x$Ga$_{1-x}$As buffer layer.[20,21] For the present situation, it is not known if the Fe on the (100) GaAs relaxes in a similar manner.

The fourth term in the free-energy expansion is the demagnetization energy for the component of magnetization perpendicular to the film plane. In the absence of a field applied perpendicularly to the film plane and if $K_1 \ll 2\pi M_s$, the magnetization is effectively forced to lie in the film plane. For bulk Fe, $K_1/M_s \simeq 275$ Oe and $4\pi M_s \simeq 21$ kOe.[22] It may be argued that these constants do not describe the thin films; however, the results of studies on Fe/GaAs systems reaffirms the validity for using these constants.[9,14,17] In addition, it was found that perpendicular anisotropy or surface anisotropy was insignificant in similar Fe/GaAs films.[14] Moreover, in the present work, the magnetic field, within experimental error, was always applied parallel to the film plane. Thus the assumption for in-plane orientation of the magnetization is well justified.

For the films studied here, the typical Kerr hysteresis curves for applied fields parallel to the $\langle 100 \rangle$ and $\langle 110 \rangle$ directions are depicted in Fig. 1. In these data the measured light intensity is proportional to the component of magnetization parallel to the applied field. For the $\langle 110 \rangle$, a magnetically intermediate direction of bulk Fe, the magnetization curve indicates an abrupt transition at 25 Oe followed by a gradual increase to saturation at approximately 550 Oe. The reversibility and slow increase of the intensity beyond the initial transition is suggestive of a rotational process. In contrast, along the $\langle 100 \rangle$, a magnetically easy direction of bulk Fe, the magnetization switches at 25 Oe directly into a saturation state. This is more in line with a domain process, particularly when one considers that the coercive field from coherent rota-
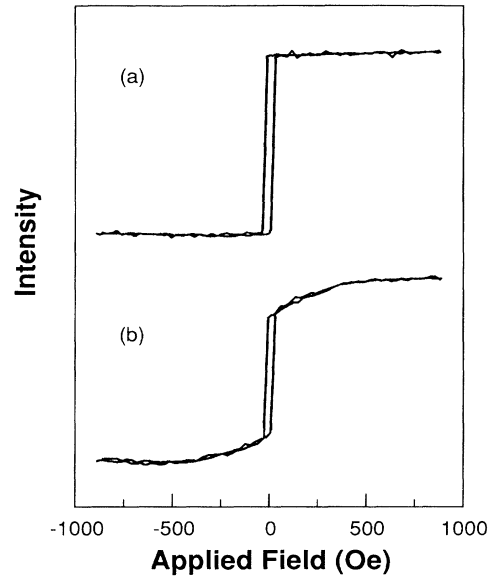

FIG. 1. Kerr hysteresis curves for applied fields parallel to the (a) $\langle 100 \rangle$ easy and (b) $\langle 110 \rangle$ intermediate axes of the crystal. For these data the measured intensity is proportional to the component of magnetization parallel to the applied field. These curves are scaled so that the saturation states are at values of $+1$ and -1 in intensity. These curves have been displaced to make comparisons easier.

tion is $2K_1/M_s \simeq 550$ Oe. These two directions are examined more closely and, at least for the reversible part of $\langle 110 \rangle$ curve, simulated via Eq. (1).

Continuing with the analysis of the free-energy expansion, denoting θ_m as the angle between the magnetization vector and the [100] axis and θ_H as the angle that the applied field makes with the [100] axis, Eq. (1) simplifies to

$$\varepsilon(\theta_m) = \kappa_1 \cos^2\theta_m \sin^2\theta_m + \kappa_u \sin^2(\pi/4 + \theta_m)$$
$$- H \cos(\theta_H - \theta_m) , \qquad (2)$$

where $\kappa_1 = K_1/M_s$, $\kappa_u = K_u/M_s$, and $\varepsilon = E/M_s$. The absence of K_2 is a result of the (100) orientation of the film plane. With this plane the direction $\cos\alpha_3 = 0$, and as a result, the sixth-order anisotropy term drops out. Toward the goal of modeling the hysteresis curves, certain generalizations for κ_1 and κ_u in Eq. (2) can be deduced directly from Fig. 1. The fact that the $\langle 110 \rangle$ direction is magnetically harder than the $\langle 100 \rangle$ places restrictions on the possible values of κ_1 and κ_u. For the above condition, κ_1 must be positive and greater than the magnitude of κ_u. For the direction of κ_u, if the axis is fixed along a particular $\langle 110 \rangle$ direction, then the sign of κ_u can be either positive or negative. However, the same results occur if κ_u remains positive, but the axis is allowed to move to either in-plane $\langle 110 \rangle$ direction. For this model the axis of κ_u is defined, while the sign is allowed to vary. Returning to the implications of Fig. 1, as a result of the $\kappa_u < \kappa_1$ condition, for $\kappa_u = 0$ and no applied field, it can be shown from Eq. (2) that the $\langle 110 \rangle$-type axes are unstable directions

for the magnetization, while the ⟨100⟩ are the stable directions. However, when $0 < \kappa_u < \kappa_1$, the stable direction for the magnetization moves an angle of $0.5 \sin^{-1}(\kappa_u / \kappa_1)$ from the ⟨100⟩ direction toward the ⟨110⟩, while the unstable directions remain the ⟨110⟩. Thus, for $\kappa_u / \kappa_1 \sim 20\%$, the easy axes move $\sim 5°$ from the ⟨100⟩ toward the ⟨110⟩ directions. The uncertainty in the angular measurements for the data presented here is about $2°$, so that this effect of κ_u may not be noticeable.

B. Magneto-optics

A measurement of the Kerr effect involves shining polarized light on a ferromagnet and subsequently allowing the reflected light to pass through an analyzer before detection. Within this context it is important to understand how the measured intensity depends upon the polarization of the incident light, analyzer angle, and orientation of the magnetization relative to the plane of incidence. Here we mention only the very basic points; the reader is encouraged to review the many articles on the magneto-optical Kerr effect for a more detailed analysis.[23,24] For in-plane magnetization, the magneto-optical Kerr effects are classified into the transverse and longitudinal geometries. In the transverse Kerr effect, the magnetization is perpendicular to the plane of incidence, while in the longitudinal effect, the magnetization is parallel to the plane of incidence. It has been previously shown[15] that the light intensity, after passing through the analyzer, which is oriented at an angle of $+\theta_a$ from the plane of incidence, is given by

$$I/I_0 = |m_l^2 r_{pp}^l + m_t^2 r_{pp}^t|^2 \cos^2\theta_a$$

$$+ |m_l^2 r_{sp}^l|^2 \sin^2\theta_a - [(m_l^2 r_{pp}^l + m_t^2 r_{pp}^t)m_l^2 r_{ps}^{l*}$$

$$+ \text{c.c.}]\cos\theta_a \sin\theta_a , \quad (3)$$

where in this expression $m_l = M_l / M_s$, $m_t = M_t / M_s$, and the polarizer is oriented so that the incident light is polarized in the plane of incidence. M_l and M_t are the components of magnetization parallel and perpendicular to the plane of incidence, respectively. The terms such as r_{sp}^l are the Fresnel reflection coefficients, which depend upon the index of refraction n, magneto-optical constant Q, and angle of incidence of the polarized light.[24] As an example and to underscore the sensitivity of the measured signal to the analyzer angle θ_a, and therefore the two components of the magnetization, Figs. 2 and 3 depict the analyzer dependence for when the applied field is nearly parallel to a ⟨110⟩ direction. As is quite apparent in these curves, the reversible part of the magnetization curve in Fig. 2(a) actually has a second irreversible transition occurring at 250 Oe [see Figs. 2(b) and 2(c)]. The sensitivity to this transition increases as the analyzer is rotated toward extinction, up to the extent that the first transition is no longer present when $\theta_a \simeq 90°$ or $-90°$, as in Fig. 3(c). From Eq. (3) one can see that for $\theta_a = 0°$ only the component perpendicular to the plane of incidence is detected,[25] and for $\theta_a = 90°$ the component parallel to the plane of incidence is sensed. As a final comment about the qualitative comparison between Eq. (3) and Figs. 2
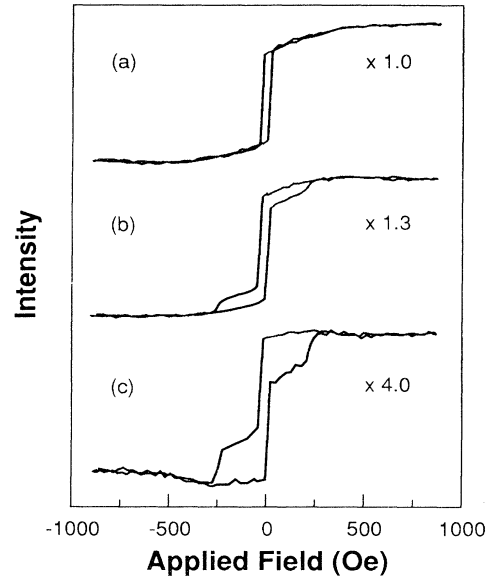

FIG. 2. Kerr hysteresis curves for applied fields parallel to the ⟨110⟩ intermediate axes. The incident light is polarized in the plane of incidence and the analyzer is at angles of (a) $\theta_a = 0°$, (b) $\theta_a = 30°$, and (c) $\theta_a = 60°$ from the plane of incidence. The curve for $\theta_a = 0°$ is scaled to bring the $+M_s$ and $-M_s$ saturation states to values of $+1$ and -1, respectively. The other data are scaled relative to this curve and displaced to make comparisons easier. A positive analyzer angle is defined as a counterclockwise rotation of the analyzer transmission axis relative to the plane of incidence when viewing toward the light source.
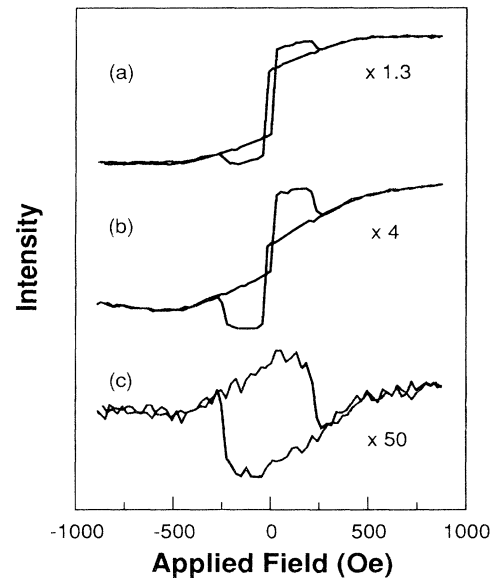

FIG. 3. Kerr hysteresis curves for the same conditions as in Fig. 2 except the analyzer angles are now at (a) $\theta_a = -30°$, (b) $\theta_a = -60°$, and (c) $\theta_a = -85°$ from the plane of incidence. A negative analyzer angle is defined as a clockwise rotation of the analyzer transmission axis relative to the plane of incidence when viewing toward the light source.

and 3, note that even up to $\theta_a = 60°$ the saturation-to-saturation intensity difference follows a $\cos^2\theta_a$ dependence (the multiplication factor next to each curve, which is used to bring the intensity change between saturation states to the same value, varies as $1/\cos^2\theta_a$), indicating that the first term in Eq. (3) dominates in the saturation regime at these analyzer angles.

As remarked before, the Fresnel reflection coefficients depend upon the index of refraction n and the magneto-optical parameter Q of Fe. A knowledge of these constants for $\lambda = 6328$ Å is necessary in order to model the Kerr hysteresis curves using Eq. (3). For this analysis the values obtained in other studies of the optical properties of Fe are used.[26-31] The variation in the values of the index of refraction from these studies are partly due to the diverse preparation methods of the metal films, the presence of oxide layers, and the different measurement techniques. Generally, the values obtained with oxide-coated films are less than those without oxides. As pointed out by Johnson and Christy,[27] the effect of a thin oxide layer, transparent or absorbing, is always to reduce the reflectance of a bare metal. The films here are also oxide coated,[32] and as a result, it is found that these data are best represented by the values determined from oxide-coated films,[29] where $n = 1.79 + i2.57$ and $Q = 0.01 + i0.004$. Utilization of the other published values of n and Q does not change the general features of the simulated curves, but appears only to vary the saturation-to-saturation intensity difference, effectively a scale factor.

In Eq. (3) both the $\cos^2\theta_a$ and $\sin\theta_a \cos\theta_a$ terms have prefactors with linear and quadratic dependencies on the magnetization (see Appendix for details). For the values of n and Q that best represent the data, these quadratic terms in the magnetization are at least two orders of magnitude smaller than the linear terms. This remains true for the other referenced values of n and Q. Furthermore, the $\sin^2\theta_a$ term is significant only for analyzer angles near extinction; for example, when $\theta_a \simeq 89.5°, 0.5°$ from extinction, this term (including prefactor) contributes approximately 6% of the total intensity. Further from extinction the contribution from this term rapidly diminishes. Thus, by dropping the quadratic terms, the $\cos^2\theta_a$ and $\sin\theta_a \cos\theta_a$ terms remain, and in terms of the magnetization components, Eq. (3) simplifies to

$$I/I_0 = (A + BM_t/M_s)\cos^2\theta_a + (CM_l/M_s)\sin\theta_a \cos\theta_a \ ,$$

(4)

where the constants A, B, and C depend upon the index of refraction n, magneto-optical constant Q, and angle of incidence of the polarized light. The details of the calculations arriving at Eq. (4) are given in the Appendix.

IV. EXPERIMENTAL RESULTS

A. Hysteresis for H parallel to the $\langle 100 \rangle$ directions

The Kerr hysteresis curves for an applied field parallel to a $\langle 100 \rangle$ direction appear in Fig. 4. The important observation concerning these curves is the absence of any
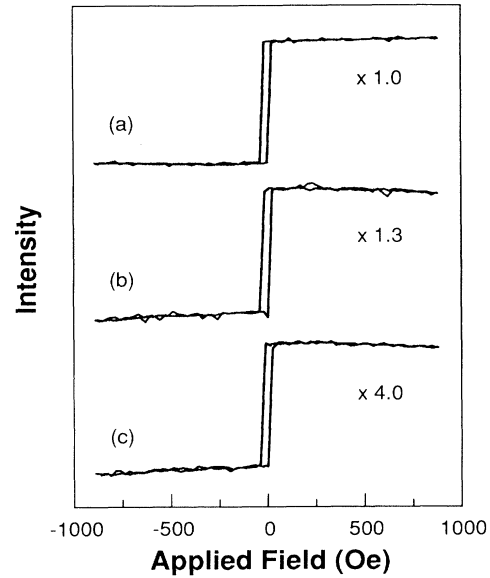

FIG. 4. Kerr hysteresis curves for the applied field parallel to a $\langle 100 \rangle$ easy axis. Depicted here are curves for analyzer angles of (a) $\theta_a = 0°$, (b) $\theta_a = 30°$, and (c) $\theta_a = 60°$. The hysteresis curve for $\theta_a = 0°$ is scaled so that the $+M_s$ and $-M_s$ saturation states are $+1$ and -1, respectively. The other data are scaled relative to this curve and displaced for easier comparisons.

analyzer dependence such as that for the $\langle 110 \rangle$ directions. The only dependence on the analyzer angle here is the simple $\cos^2\theta_a$ intensity variation due to the crossing of the analyzer and polarizer, the first term in Eq. (4). This simple dependence on the analyzer angle continues down to angles near extinction. This implies that only a single component of the magnetization is detected in these curves. Furthermore, the coercivity for this loop is 25 Oe. For a rotational process, the reversal field, for bulk Fe constants, is $2K_1/M_s \simeq 550$ Oe. These two points, single-component loop and small reversal field, imply that domain nucleation or unpinning of 180° domains is the likely mechanism for this magnetization reversal. If the transition is due to the unpinning of domains, simplistic arguments[33] suggest that the coercive field should vary as $H_0/\cos\theta$ as the applied field is rotated to an angle θ from the $\langle 100 \rangle$ easy axis. It is found, however, that a rotation of the magnetic field from the $\langle 100 \rangle$ directions induces an entirely different reversal, not just a simple adjustment of the coercive field. For the case when the applied field is within 2.5° of the $\langle 100 \rangle$ directions, the magnetization process now occurs in two steps, an initial transition at approximately 10 Oe and a second transition at 25 Oe. Additional details about this two-state reversal and how it depends upon the orientation of the applied magnetic field are discussed in the next section.

B. Hysteresis for H parallel to the $\langle 110 \rangle$ directions

For these films the magnetization process for a magnetic field nearly parallel to the $\langle 110 \rangle$ direction is consider-

ably more complex than that of the $\langle 100 \rangle$ direction. Examples of these Kerr hysteresis curves are depicted in Figs. 2 and 3. The presence of the second transition cannot be adequately accounted for by a simple domain-wall process. A somewhat similar difference between the $\langle 10 \rangle$ and $\langle 11 \rangle$ curves has been seen by Zhong et al.[34] in ultrathin Ni-Fe bilayers. For these data [e.g., Fig. 3(a)] after saturation at 900 Oe, the magnetization remains saturated along the applied field until approximately 550 Oe. As the field decreases further, the intensity gradually diminishes until, at -25 Oe, the magnetization undergoes an irreversible transition. Here the component perpendicular to the plane of incidence (parallel to the applied field) changes sign. This conclusion can be supported by searching for any changes in the magnetization component perpendicular to the applied field. In Fig. 3(c) the analyzer is rotated to near extinction; this is the condition for detection of the component perpendicular to the applied field.

The data in Fig. 3(c) were taken with $\theta_a = -85°$ for which $\cos^2\theta_a / \cos\theta_a \sin\theta_a \simeq 10\%$. The ratio B/C in Eq. (4) is about 2 for the values of n and Q referenced in Sec. II. As a result, the response to the component perpendicular to the applied field is greater than the component parallel to the applied field. No transition, up to the sensitivity of the equipment, appears in these loops near -25 Oe, suggesting that the component parallel to the applied field is responsible for the transition.[35] By increasing the applied field in the $-\mathbf{H}$ direction, a second transition occurs at -250 Oe. This transition is a result of the component perpendicular to the applied field. The light intensity monitored in Fig. 3(c) has a maximum sensitivity to the component of magnetization perpendicular to the applied field, whereas in Fig. 2(a) the sensitivity to the component parallel to the applied field dominates. Comparing these two leads one to conclude that the transition at -250 Oe involves the magnetization component perpendicular to the applied field. An additional increase in the applied field in the $-\mathbf{H}$ direction causes the magnetization to saturate in the direction of the applied field.

V. MODEL RESULTS

In the single-domain model with coherent rotation of the magnetization, the angle θ_m that minimizes the free energy, i.e., Eq. (2), can be calculated. However, for nonzero applied fields, it is intractable to find an analytic solution for the magnetization angle. Instead, this nonlinear equation is numerically solved to find the lowest-energy configuration for a specific applied field H. For a given initial magnetization direction, e.g., saturation state, the subsequent direction of $\mathbf{M}$, the local minimum, is a function of H and satisfies the conditions that $\partial\varepsilon/\partial\theta_m = 0$ and $\partial^2\varepsilon/\partial\theta_m^2 > 0$. The modeled hysteresis loops are a result of tracking this local minimum as a function of H.

If the saturation field is along a crystal direction, an ambiguity is present as to which direction the magnetization will rotate to when the applied field is reduced. Experimentally, this ambiguity generally does not develop. The most likely reason for this is that it is difficult to per-

fectly align the applied magnetic field with a crystal axis. Therefore, in the model, a small misalignment of the applied field is introduced in order to induce the magnetization to rotate toward a particular direction. In the course of the rotation, for certain values of the applied field, an inflection point in the free energy develops, characterized by $\partial\varepsilon/\partial\theta = \partial^2\varepsilon/\partial\theta^2 = 0$, and the magnetization undergoes an irreversible change in orientation. Physically, this corresponds to the magnetization overcoming the energy barrier between local minima of the anisotropy energies of the material. In terms of the simulated hysteresis loops, these transitions, if only one transition is present, denote the coercive field. For two transitions, as in the $\langle 110 \rangle$ curves, the first transition nearest 0 Oe is denoted H_{c1} and the second is denoted H_{c2}.

An example of the results from the simulation with $\theta_H = 44°$, $\kappa_1 = 195$ Oe, and $\kappa_u = 20$ Oe, which gives the best fit, are compared to the experimental curves in Figs. 5 and 6. There is good agreement between the data and simulations. The agreement is equally good for the other curves of Figs. 2 and 3. This indicates that the direction of the magnetization vector as a function of the applied field is correctly reproduced.

The agreement of the model with the data implies that the reversal process occurs in the following manner. Starting from saturation along the $\langle 110 \rangle$ direction, the magnetization rotates reversibly to the nearest easy axis as the applied field is reduced to 0 Oe (recall that the applied field is slightly disoriented from the $\langle 110 \rangle$; thus one of the two easy axes that are $45°$ from the $\langle 110 \rangle$ is closer to the saturation position of the magnetization). Increasing the field in the $-\mathbf{H}$ direction causes the component parallel to the applied field to reverse direction at -25 Oe. The longitudinal component continues to have the
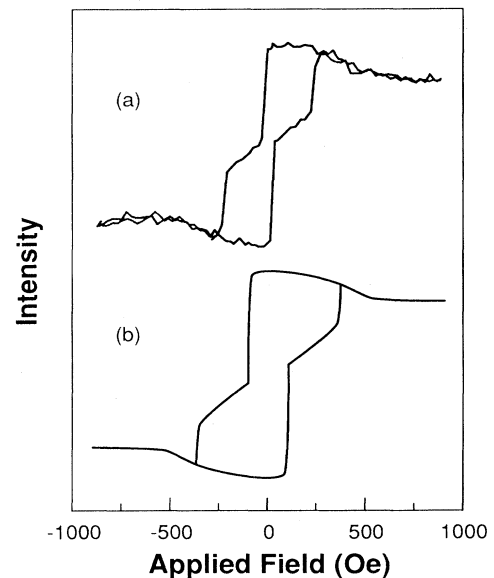

FIG. 5. Comparison of the experimental Kerr hysteresis curve in (a) with the simulation in (b) for an analyzer angle of $\theta_a = -75°$. For the simulated curves here and in Fig. 6, $n = 1.79 + i2.57$, $Q = 0.01 + i0.004$, $\theta_H = 44°$, $\kappa_1 = 195$ Oe, and $\kappa_u = 20$ Oe.
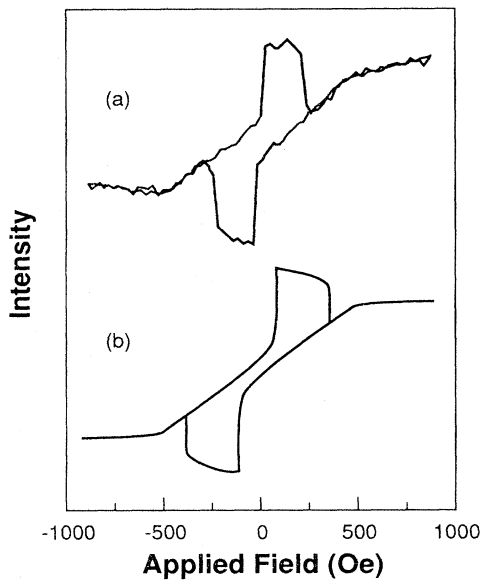
FIG. 6. Comparison of the experimental curve in (a) with the simulation in (b) for an analyzer angle of $\theta_a = +75°$. The curves have been displaced to make comparisons easier.

same sign. Between -25 and -250 Oe there is a resumption of the rotation, as can be seen in the curves by the small intensity variation. Increasing the applied field further in the $-H$ direction induces the component perpendicular to the applied field to change sign at -250 Oe. An additional increase of the magnetic field in the $-H$ direction above -250 Oe causes the magnetization to rotate into the direction of the applied field until saturation.

The overshoots appearing in the Kerr hysteresis curves, for certain analyzer angles, are a result of the independent switching of the two magnetization components which give separate contributions to the total detected intensity. The amount that each component contributes varies with the analyzer angle and is expressed in Eq. (4). Note that the sign of the M_l/M_s term, which determines if an undershoot or overshoot will be present, can be changed by careful selection of the analyzer angle.[15]

Even though the qualitative agreement is good, there are some aspects of the simulations that require more extensive discussion. First, as noted previously, the transition fields of the modeled loops are in poor agreement with the data. It is found that the parameters κ_1 and κ_u cannot be adjusted to obtain simultaneously the correct switching and saturating fields. As an example, the two switching fields can be reduced to the correct values with very low values of the parameters, $\kappa_1 \simeq 80$ Oe and $\kappa_u \simeq 60$ Oe, but the saturation field is reduced to 280 Oe. From Eq. (2) it can be shown that the saturation fields goes as $2(\kappa_1 + \kappa_u)$. Previous work with these samples did not indicate that κ_1 should have an anomalously low value.[36] On the other hand, bulk values of $\kappa_1 = 275$ Oe and $\kappa_u = 0$ Oe reproduce the saturation field, but the first and second reversal fields are increased to 155 and 465 Oe, respec-

tively. The answer to this inconsistency almost certainly lies in the original assumption that the system remains as a single domain during the irreversible transitions. It should be noted that these values of κ_1 and κ_u are lower than those found by Krebs, Jonker, and Prinz[14] ($\kappa_1 = 225$ Oe and $\kappa_u = 40$ Oe); however, for this study, $\kappa_u = 10\%$ of κ_1, which is approximately the same percentage as in the FMR investigation. Furthermore, as far as the magnetization process is concerned, the effect of the uniaxial anisotropy was insignificant. This is not entirely unexpected since κ_u is at most only about 10% of the cubic anisotropy.

Second, the magnetization, during its reversal process, follows the local minimum rather than the global minimum. If the magnetization made a transition to the global minimum, this unique process would not appear. This observation and the previous suggest that the irreversible transitions occur by the nucleation or unpinning of 90° domains at the two transitions fields. In order to check if residual domains[37] were present, these samples were subjected to an in-plane field of 10 kOe. The magnitude of the reversal fields did not change even after the application of these large fields. However, as in the work done by Fowler, Fryer, and Treves[38] on Fe whiskers, sharp edges in the sample may allow domains to be present even at fields of this order of magnitude. The value of the first transition field may imply that the unpinning or nucleation of domains for the easy axis is the same as the intermediate direction. Calculations of the nucleation field due to inclusions yield nucleating fields of 10 Oe and less, depending upon the size of the inclusion.[39] The dependence of these nucleating fields on the direction of the applied field also varies as $1/\cos\theta$, similar to that in the unpinning argument. Thus angular measurements of the transition fields may not be able to differentiate between the two mechanisms. It is important to note that in most calculations involving unpinning or nucleation of domains, only a simple uniaxial anisotropy is assumed. Here the anisotropy is cubic, which may change the angular dependence of the nucleation fields.

Plotted in Fig. 7 are the angular dependences of the first transition field H_{c1} and the second transition field H_{c2}. For the scale of Fig. 7, $H_0/\cos\theta$ is essentially a straight line for the range of angles that the data spans. Thus one cannot rule out domain unpinning or nucleation for H_{c1}. On the other hand, the second transition field H_{c2} depends strongly on the direction of the applied magnetic field. This angular dependence cannot be explained by the simple $H_0/\cos\theta$ relation. Also plotted in this figure are the predicted angular dependences of H_{c1} and H_{c2} from the rotation model with $\kappa_1 = 195$ Oe and $\kappa_u = 20$ Oe. For angles far from the easy axis, the angular dependence of H_{c2} does follow the general trend of the data. Furthermore, in this simplistic model, this change of reversal mechanism from a single irreversible transition to two irreversible transitions near the $\langle 100 \rangle$ directions appears as a natural consequence of the magnetization following the local minima in a cubic anisotropy field; there are now two energy barriers to overcome when the applied field is disoriented from the $\langle 110 \rangle$ directions.
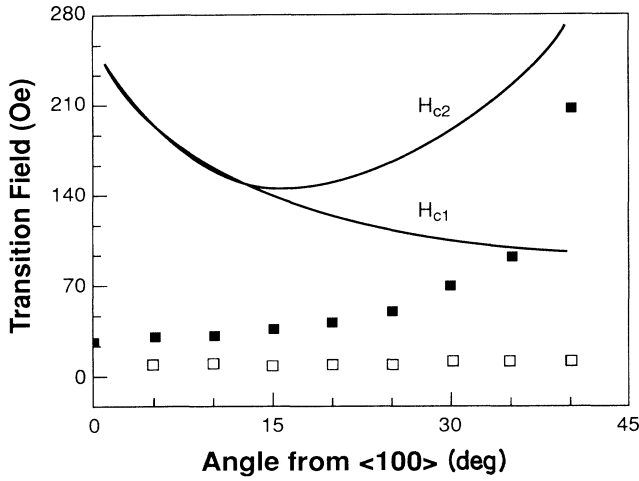
FIG. 7. Angular dependence of the two transition fields H_{c1} (□) and H_{c2} (■), as the applied magnetic field is rotated between a $\langle 100 \rangle$ and $\langle 110 \rangle$. The error bars for the angle of the magnetic and transition fields are equal to the width of the data symbols. The solid lines labeled H_{c1} and H_{c2} are the angular dependence of the transition fields predicted by the rotation model for $\kappa_1 = 195$ Oe and $\kappa_u = 20$ Oe.

VI. SUMMARY AND CONCLUSIONS

From the preceding discussion, and as one would anticipate, it is quite clear that the uniform rotation model cannot explain all the details of the magnetization process in these Fe/GaAs (100) films. However, this simple model provides valuable insight into the reversal processes occurring for applied fields near the $\langle 110 \rangle$ directions. Clearly, as is shown experimentally and in the simulations, the ideal rotation and irreversible transitions that one conventionally thinks of will occur for the special case of when the applied field is aligned with the $\langle 110 \rangle$ direction. In a more realistic situation when the applied field is disoriented from the $\langle 110 \rangle$ direction, because of either experimental uncertainty of the direction of the applied field or a mosaic structure of the single crystal, a simple adjustment of the coercive field does not adequately explain these data. The reversal now proceeds through an entirely different mechanism, and it is argued that this process occurs by the nucleation or unpinning of two 90° domains at distinct transition fields. Interesting overshoots and undershoots that appear in this and in other studies of the Kerr effect of single-crystal systems can be attributed to the appearance of more than one Kerr effect. Here the novel curves are the result of the presence of both the longitudinal and transverse Kerr effects. The proper combination of these two effects as illustrated in this study can account for the overshoots and undershoots as well as the general analyzer dependence seen in the data.

With simulations incorporating this combination of Kerr effects and the simple rotation model for the magnetization, other single-crystal systems can be studied in

more detail than is possible with a single-component measurement system. Here we have shown that this method can provide valuable insight into the reversal mechanism occurring in Fe/GaAs (100) single-crystal films that would not have ordinarily been expected to occur.

ACKNOWLEDGMENTS

APPENDIX

The Fresnel reflection coefficients for the transverse and longitudinal Kerr effects listed here are only approximate; terms higher than order Q are neglected.[24,40] Furthermore, the film thickness is assumed to be large compared to the skin depth at $\lambda = 6328$ Å. These assumptions do have justification in the present analysis. First, the experimental values of Q typically have $|Q| \leq 0.03$, so that the first assumption is warranted. Second, studies done by Moog et al.[41] suggest that a "bulk" Kerr effect appears for approximately 130 Å of Fe on Au, the typical Fe thicknesses used here are 100–150 Å. Finally, it should be pointed out that the presence of an oxide layer is not explicitly taken into account in the reflection coefficients. The oxide is only indirectly addressed through the value of the index of refraction for the Fe film.

First, the appropriate Fresnel reflection coefficients are listed. The reflection coefficients for the transverse Kerr effect are

$$r_{pp}^t = \frac{n\beta - \beta'}{n\beta + \beta'}\left[1 + \frac{\kappa_2 \sin(2\theta)}{n^2(n^2 \cos^2\theta - 1) + \sin^2\theta}\right], \quad \text{(A1)}$$

$$r_{ss}^t = \frac{\beta - n\beta'}{\beta + n\beta'}, \quad \text{(A2)}$$

$$r_{ps}^t = r_{sp}^t = 0. \quad \text{(A3)}$$

In the above θ is the angle of incidence measured from the sample normal, n is the index of refraction of the material, $\beta = \cos\theta$, $\beta' = [1 - (\sin^2\theta)/n^2]^{1/2}$, and $\kappa_2 = in^2Q$ is the off-diagonal component of the relative permittivity tensor. The coefficients for the longitudinal Kerr effect are

$$r_{pp}^l = \frac{n\beta - \beta'}{n\beta + \beta'}, \quad \text{(A4)}$$

$$r_{ss}^l = \frac{\beta - n\beta'}{\beta + n\beta'}, \quad \text{(A5)}$$

$$r_{ps}^l = -r_{sp}^l = \frac{\gamma\beta\kappa_2}{n^2\beta'(n\beta + \beta')(\beta + n\beta')}, \quad \text{(A6)}$$

where $\gamma = \sin\theta$.

Presently, the constants A, B, and C appearing in Eq. (4) are computed using the above coefficients and Eq. (3). From the first term in Eq. (3),

$$m_l^2 r_{pp}^l + m_t^2 r_{pp}^t = m_l^2 \frac{n\beta - \beta'}{n\beta + \beta'} + m_t^2 \frac{n\beta - \beta'}{n\beta + \beta'} \left[1 + \frac{in^2 Q \sin(2\theta)/m_t}{n^2(n^2 \cos^2\theta - 1) + \sin^2\theta} \right] . \tag{A7}$$

Given that the magnetization is restricted to move in the film plane, the components of magnetization relative to the plane of incidence of the light beam can be found from geometry to be $M_t = M_s \sin(\pi/4 + \theta_m)$ and $M_l = M_s \cos(\pi/4 + \theta_m)$, where θ_m is the angle between the magnetization and plane of incidence. As a result, (A7) can be further simplified by noting that $m_l^2 + m_t^2 = (M_l/M_s)^2 + (M_t/M_s)^2 = 1$. Thus the reduced expression is

$$\frac{n\beta - \beta'}{n\beta + \beta'} \left[1 + \frac{in^2 Q \sin(2\theta) m_t}{n^2(n^2 \cos^2\theta - 1) + \sin^2\theta} \right] . \tag{A8}$$

Multiplying (A8) by its complex conjugate and simplifying the resulting expression, it is found that the first term in Eq. (3) is

$$\left| \frac{n\beta - \beta'}{n\beta + \beta'} \right|^2 \left[1 + \left[\frac{in^2 Q \sin(2\theta)}{n^2(n^2 \cos^2\theta - 1) + \sin^2\theta} + \text{c.c.} \right] \frac{M_t}{M_s} + \frac{|n|^4 |Q|^2 m_t^2 \sin^2 2\theta}{[n^2(n^2 \cos^2\theta - 1) + \sin^2\theta][n^{2*}(n^{2*} \cos^2\theta - 1) + \sin^2\theta]} \right] . \tag{A9}$$

Dropping the term that is quadratic in the magneto-optical parameter Q, one can define

$$A \equiv \left| \frac{n\beta - \beta'}{n\beta + \beta'} \right|^2 \tag{A10}$$

and

$$B \equiv \left| \frac{n\beta - \beta'}{n\beta + \beta'} \right|^2 \left[\frac{in^2 Q \sin(2\theta)}{n^2(n^2 \cos^2\theta - 1) + \sin^2\theta} + \text{c.c.} \right] , \tag{A11}$$

such that the first term in Eq. (3) is $(A + BM_t/M_s)\cos^2\theta_a$.

The third term in Eq. (3), the $\cos\theta_a \sin\theta_a$ term, is

$$-[(m_l^2 r_{pp}^l + m_t^2 r_{pp}^t)m_l^2 r_{ps}^{l*} + \text{c.c.}]$$

$$= \frac{n\beta - \beta'}{n\beta + \beta'} \left[1 + \frac{in^2 Q m_t \sin(2\theta)}{n^2(n^2 \cos^2\theta - 1) + \sin^2\theta} \right] \left[\frac{in^{2*} Q^* \gamma \beta m_l}{n^{2*} \beta'^*(n^*\beta + \beta'^*)(\beta + n^*\beta'^*)} \right] + \text{c.c.} \tag{A12}$$

Simplifying this quantity, we obtain

$$\frac{n\beta - \beta'}{n\beta + \beta'} \left[\left[\frac{in^{2*} Q^* \gamma \beta m_l}{n^{2*}\beta'^*(n^*\beta + \beta'^*)(\beta + n^*\beta'^*)} \right] + \frac{|n|^4 |Q|^2 \gamma \beta m_l m_t \sin(2\theta)}{(n^2(n^2 \cos^2\theta - 1) + \sin^2\theta)(n^{2*}\beta'^{2*}(n^*\beta + \beta'^*)(\beta + n^*\beta'^*))} \right] + \text{c.c.} \tag{A13}$$

Again, by dropping the $|Q|^2$ term, the third term can be expressed as CM_l/M_s with C defined as

$$C \equiv \frac{n\beta - \beta'}{n\beta + \beta'} \left[\frac{in^{2*} Q^* \gamma \beta}{n^{2*}\beta'^*(n^*\beta + \beta'^*)(\beta + n^*\beta'^*)} \right] + \text{c.c.} \tag{A14}$$

The second term in Eq. (4) is to lowest order, quadratic in the magneto-optical parameter Q. Thus this term is insignificant for angles away from $\theta_a = 90°$.

[1]K. Honda and S. Kaya, Sci. Rep. Tohoku Imperial Univ. **15**, 721 (1926).

[2]E. P. Wohlfarth, in *Ferromagnetic Materials*, edited by E. P. Wohlfarth (North-Holland, Amsterdam, 1980), Vol. 1.

[3]R. M. Bozorth, *Ferromagnetism* (Van Norstrand, New York, 1951).

[4]E. C. Stoner and E. P. Wohlfarth, Philos. Trans. R. Soc. A **240**, 599 (1948).

[5]M. E. Schabes and H. N. Bertram, J. Appl. Phys. **64**, 1349 (1988).

[6]C. E. Johnson and W. F. Brown, J. Appl. Phys. **32**, 243S (1961).

[7]K. B. Hathaway and G. A. Prinz, Phys. Rev. Lett. **47**, 1761 (1981).

[8]G. A. Prinz and J. J. Krebs, Appl. Phys. Lett. **39**, 397 (1981).

[9]K. T. Riggs, E. Dan Dahlberg, and G. A. Prinz, Phys. Rev. B **41**, 7088 (1990).

[10]G. A. Prinz, in *Thin Film Growth Techniques for Low-Dimensional Structures*, edited by R.F.C. Farrow, S. S. Parkin, P. J. Dobson, J. H. Neave, and A. S. Arrott, NATO Advanced Research Workshop of Thin Film Growth Tech-

niques for Low-Dimensional Structures (Plenum, University of Sussex, Brighton, United Kingdom, 1986), Vol. 163, p. 311.

[11]K. T. Riggs, E. Dan Dahlberg, and G. A. Prinz, J. Magn. Magn. Mater. **73**, 46 (1988).

[12]J. J. Krebs, F. J. Rachford, P. Lubitz, and G. A. Prinz, J. Appl. Phys. **53**, 8058 (1982).

[13]G. A. Prinz, G. T. Rado, and J. J. Krebs, J. Appl. Phys. **53**, 2087 (1982).

[14]J. J. Krebs, B. T. Jonker, and G. A. Prinz, J. Appl. Phys. **61**, 2596 (1987).

[15]J. M. Florczak and E. Dan Dahlberg, J. Appl. Phys. **67**, 7520 (1990).

[16]Sushin Chikazumi, *Physics of Magnetism* (Wiley, New York, 1964), Chap. 14.

[17]M. Rubinstein, F. J. Rachford, W. W. Fuller, and G. A. Prinz, Phys. Rev. B **37**, 8689 (1988).

[18]Ernst Schlomann, J. Appl. Phys. **41**, 1617 (1970).

[19]R.F.C. Farrow, S. S. Parkin, V. S. Sperious, C. H. Wilts, R. B. Beyers, P. Pitner, J. M. Woodall, S. L. Wright, P. D. Kirchner, and G. D. Pettit, in *Epitaxy of Semiconductor Layered Structures,* edited by R. T. Tung, L. R. Dawson, and R. L. Gunshor, Materials Research Society Symposium Proceedings No. 102 (Material Research Society, Pittsburgh, 1988), p. 483.

[20]P. J. Orders and B. F. Usher, Appl. Phys. Lett. **50**, 980 (1987).

[21]K. L. Kavanagh, M. A. Capano, L. W. Hobbs, J. C. Barbour, P.M.J. Maree, W. Schaff, J. W. Mayer, D. Pettit, J. M. Woodall, J. A. Stroscio, and R. M. Feenstra, J. Appl. Phys. **64**, 4843 (1988).

[22]B. D. Cullity, *Introduction to Magnetic Materials* (Addison-Wesley, Reading, MA, 1972), pps. 234 and 617.

[23]A. V. Sokolov, *Optical Properties of Metals* (Elsevier, New York, 1968), Chap. 10.

[24]Marvin J. Freiser, IEEE Trans. Magn. MAG-4, 152 (1967).

[25]The Fresnel coefficient r_{pp}^{l} is independent of any magnetization component up to order Q in the magneto-optical con-

stant. However, r_{pp}^{t} depends upon M_{t}/M_{s}, the component perpendicular to the plane of incidence.

[26]J. Kranz and H. Stremme, IEEE Trans. Magn. MAG-5, 453 (1969).

[27]P. B. Johnson and R. W. Christy, Phys. Rev. B **9**, 5056 (1974).

[28]M. N. Deeter and D. Sarid, Appl. Opt. **28**, 2911 (1989).

[29]M. Corke, A.W.J. Dawkins, and R. B. Inwood, J. Phys. E **15**, 251 (1982).

[30]H. T. Yolken and J. Kruger, J. Opt. Soc. Am. **55**, 842 (1965).

[31]J. H. Judy, J. K. Alstad, G. Bate, and J. R. Wiitala, IEEE Trans. Magn. MAG-4, 401 (1968).

[32]A. J. Malmed and J. J. Carroll, J. Vac. Sci. Technol. **10**, 164 (1973).

[33]M. Kersten, Z. Angew. Phys. **7**, 313 (1956); **8**, 382 (1956); **8**, 496 (1956).

[34]Q. M. Zhong, A. S. Arrott, B. Heinrich, and Z. Celinski, J. Appl. Phys. **67**, 4448 (1990).

[35]This can also be checked by removing the analyzer. In this circumstance the intensity only has a quadratic term in M_{l}/M_{s}, but both linear and quadratic terms in M_{t}/M_{s}. The quadratic terms are at least two orders of magnitude smaller than the linear term. As a result, the detected intensity is predominately sensitive to the component of magnetization parallel to the applied field. For this "no analzyer" case, the $\theta_{a}=0°$ hysteresis curve is reproduced, confirming the original observation.

[36]D. K. Lottis, J. Florczak, E. Dan Dahlberg, S. Batra, A. M. Wowchak, and P. I. Cohen, J. Appl. Phys. **63**, 3662 (1988).

[37]Amikham Aharoni, Rev. Mod. Phys. **34**, 227 (1962).

[38]C. A. Fowler, Jr., E. M. Fryer, and D. Treves, J. Appl. Phys. **32**, 296S (1961).

[39]J. Goodenough, Phys. Rev. **95**, 917 (1954).

[40]G. Metzger, P. Pluvinage, and R. Torguet, Ann. Phys. (Paris) **10**, 5 (1965).

[41]E. R. Moog, C. Liu, S. D. Bader, and J. Zak, Phys. Rev. B **39**, 6949 (1989).